ARTICLE NO. 78-1277R

Dispersed Fly-by-Wire Sensor System for Improved Combat Survivability

Howard Berman* and Jean Boudreau†
Grumman Aerospace Corporation, Bethpage, N.Y.

Recent developments in digital fly-by-wire flight control technology can offer improved survivability for combat aircraft. Redundancy, which is used to achieve the desired levels of reliability and failure tolerance, can also lead to decreased vulnerability. Results are presented to show that sensor dispersion, in combination with analytic redundancy techniques, can enhance flight control system survivability. However, dispersion of flight control sensors, e.g., gyros and accelerometers, can cause problems in sensor redundancy management and in control law dynamic performance. It is shown that these problems, which are due to like sensors measuring different elastic motions and rigid-body kinematic effects, can be eliminated by using state estimators to remove the effects from the sensor data.

Introduction

MANY current advanced fighter/attack aircraft designs are committed to the use of redundant digital fly-by-wire (FBW) flight control systems. These aircraft designs take advantage of the flexibility and potentially high reliability of digital FBW to enable control configured vehicle (CCV) concepts to be used in the design. The CCV concepts of relaxed static stability and load control can permit increased mission payloads. Specialized control modes suited to each mission phase can increase pilot effectiveness in combat. Further improvements in mission effectiveness and safety can be achieved by dispersion of the flight control system (FCS) components to enhance survivability.

Redundancy is used in FCS design to achieve desired reliability and failure tolerance goals. Typically, it is obtained by replicating system components and using suitable failure detection and voting algorithms to prevent the use of signals from failed or damaged components. Another way to obtain redundancy is through analytic means. This paper describes how the use of redundant sensor dispersion and analytic redundancy techniques can result in enhanced flight control system survivability.

Vehicle motion sensors are normally located in the midbody area of fighter-type aircraft to minimize the body bending inputs. Even so, without care in placement, or filtering of the sensor outputs, unstable interactions of airframe elasticity with the aircraft control system can occur. For redundant systems (ignoring vulnerability considerations) it is most desirable to locate all the sensors of one type, such as normal accelerometers, as close together as possible. This prevents differing bending inputs and differing rigid-body acceleration inputs to each sensor. These effeccts can make failure detection difficult. Thus, when dispersed gyros and accelerometers are used, successful techniques must be developed to deal with the differing bending inputs and rigid-body accelerations. Removal of these unwanted motions from the dispersed sensor outputs is termed "normalization."

Presented as Paper 78-1277 at the AIAA Guidance and Control Conference, Palo Alto, Calif., Aug. 7-9, 1978; submitted Oct. 12, 1978; revision received May 10, 1979.

Index categories: Handling Qualities, Stability and Control; Military Missions.

*Senior Engineer.
†Group Leader. Member AIAA.

A requirement placed on this study was that the resulting flight control system design should be fail operational, fail operational, fail safe. The fail-safe requirement implies an immediate emergency landing capability after the third failure. In order to enable maximum design flexibility for future CCV-type aircraft, the sensor system should be designed to provide motion feedbacks after a third failure. Therefore, in effect, a three-fail operational sensor system is required, although considerably degraded performance is permissible after the third failure.

General Approach to Sensor Normalization

The concern with sensor dispersion within a flexible aircraft is two-fold. First, control interaction with the sensed flexible motion must be avoided. Second, normalization of dispersed redundant sensor signals is required to retain close tracking between like sensor outputs for failure detection and isolation. In order to accommodate widely dispersed sensors whose locations may be subject to relatively low-frequency, large-amplitude flexible motions with adverse phasing, there is a need to look beyond conventional notch filtering.

The normalization approach presented herein utilizes a reconfigurable steady-state Kalman estimator that is derived directly in digital form and will provide on-line estimates of bending as well as rigid-body states. Aside from sensor normalization, these estimates will provide values for unmeasured control system feedback signals, a source of information for analytic redundancy, plus compensation for noise corrupted measurements.

The estimates, in state variable form ($\hat{X}_K$), at the Kth interval, are given by,

$$\hat{X}_K = X^e_K + We_K \tag{1}$$

where X^e_K is an extrapolation of $\hat{X}_{K-1}$, given the control command u_{K-1}, so that

$$X^e_K = \phi \hat{X}_{K-1} + Fu_{K-1}$$

and e_K is the residual vector which is the difference between the measurements (Y_K) and an extrapolation of the estimated measurements at $K-1$, so that,

$$e_K = Y_K - M^T X^e_K$$

and W is the steady-state Kalman weighting matrix that is optimized as a function of plant dynamics, system noise, and measurement noise.

The actual flight implementation of Eq. (1) is realized by having stored constants for ϕ, F, M^T, and W as a function of flight condition (or air data). The estimator is reconfigured as a function of available measurements, i.e., unfailed sensors, by appropriately forming e_K and choosing the corresponding W. Thus, for each flight condition, there is a set of constant W matrices to accommodate each allowable set of available sensors.

Typically, the estimated state vector will be comprised of aircraft rigid-body feedback variables (e.g., ϕ, p, q, r, n_y, n_z), additional states needed to accurately describe the dynamics (e.g., actuator outputs, surface trim estimates), rotational acceleration estimates for kinematic compensation (e.g., $\dot{q}$, $\dot{p}$, $\dot{r}$), and bending mode state estimates for bending compensation. Perfect estimates would be obtained if all aircraft parameters and external disturbances were known exactly. Unfortunately, parameter uncertainties and unknowns make this improbable. The following sample problem is presented to demonstrate the relative insensitivity of the estimator and to provide some additional insight into the approach.

Sample Normalization Problem

Three gyro and normal accelerometer pairs were widely dispersed throughout a pitch plane model of the baseline aircraft (F-14). The sensor pairs were located in the nose, tail, and center of the left wing. Corresponding to a flight condition of Mach 0.85 at 23,000 ft, the fully coupled linearized pitch plane equations are given by

$$\dot{X}=\begin{bmatrix}\dot{n}_z\\ \dot{q}\\ \dot{\delta}_E\\ \dot{\xi}_1\\ \ddot{\xi}_1\\ \dot{\xi}_2\\ \ddot{\xi}_2\end{bmatrix}=\begin{bmatrix}-1.6 & 24.0 & -87.0 & -1.9 & 0.18 & -3.3 & 0.24\\ -0.45 & -1.1 & -14.0 & -0.43 & -53.0 & -0.92 & -0.008\\ & & -20.0 & & & & \\ & & & & 1.0 & & \\ -307.0 & -0.94 & 2673.0 & -1062.0 & -5.2 & 10.4 & 1.03\\ & & & & & & 1.0\\ -35.0 & -11.4 & -1734.0 & 15.2 & 0.13 & -2348.0 & -2.5\end{bmatrix}\times\begin{bmatrix}n_z\\ q\\ \delta_E\\ \xi_1\\ \dot{\xi}_1\\ \xi_2\\ \dot{\xi}_2\end{bmatrix}+\begin{bmatrix}85.7\\ 0\\ 20.0\\ 0\\ 450.0\\ 0\\ 417.0\end{bmatrix}\delta_{E_C} \tag{2}$$

and the measurements (Y_K) are

$$\begin{bmatrix}n_{zm_1}\\ n_{zm_2}\\ n_{zm_3}\\ q_{m_1}\\ q_{m_2}\\ q_{m_3}\end{bmatrix}=\begin{bmatrix}-1.01 & -1.59 & -56.0 & -2.15 & -0.013 & -62.3 & -0.072\\ 1.52 & 0.63 & -5.8 & 1.95 & -0.012 & -14.0 & -0.012\\ -0.23 & 0.06 & 16.4 & -4.6 & -0.023 & 5.9 & 0.01\\ & 1.0 & & & -0.0035 & & -0.048\\ & 1.0 & & & -0.0024 & & 0.029\\ & 1.0 & & & 0.0093 & & -0.0011\end{bmatrix}X=M^TX$$

where n_z is the rigid body normal acceleration (g) at the nominal center-of-gravity (c.g.), q is the rigid-body pitch rate (rad/s), δ_E is the elevator position (rad), ξ_i is the ith modal displacement (ft/normalized unit of length), and δ_{E_C} is the elevator command (rad).

In Eq. (2), two critical bending modes are included, both with inherent structural damping; these are the first wing symmetric mode and the first vertical fuselage mode. Note the extensive coupling between rigid and bending states. In the past, many control analyses have omitted this coupling, i.e., bending was excited by control surface motion only, with no coupling from bending to rigid-body states and vice-versa. This can lead to erroneous results, especially in the presence of external disturbances.

The measurements in Eq. (2) are formed by using the following relationships:

$$n_{zm_i}=n_z+\frac{lx_i}{32.2}\dot{q}+\frac{1}{32.2}\sum_{j=1}^{2}z_{ij}\ddot{\xi}_j$$

$$q_{m_i}=q+\sum_{j=1}^{2}\psi_{ij}\dot{\xi}_j \tag{3}$$

where lx_i is the X distance from the c.g. to the ith accelerometer (ft), z_{ij} is the jth mode shape displacement at the ith sensor location (normalized unit of length), and ψ_{ij} is the jth mode slope at the ith sensor location (normalized unit of length/ft).

Using Eq. (2) in combination with white noise for system and measurement uncertainties, the constants necessary to realize the discrete, steady-state Kalman estimator [Eq. (1)] were derived for a 10 Hz sampling frequency. In general, unless the stochastic properties of all error sources are accurately known, it is best to model the errors as uncorrelated white noise. This approach will desensitize the estimator to unmodeled errors. A functional flow diagram of the estimator is shown in Fig. 1. Given a sensor failure, the estimator is reconfigured by eliminating the associated W_i and adjusting the remaining weighting vectors using the precalculated constants for the particular available sensor configuration. In a classical sense, the resulting multi-input multi-output filter resembles a group of parallel notch filters connecting each measurement to each rigid-body estimate. Sensor normalization is inherent in the estimator design in that all sensor outputs are linearly weighted to obtain the best state estimate. In addition, failure detection/isolation can be accomplished using conventional comparison monitoring techniques on the residuals associated with like sensors.

Measurements whose frequency content are greater than the primary strip boundaries (for this example the boundary is $\omega_s/2=31.4$ rad/s) will be folded within the primary strip to appear as signals whose damped natural frequency is given by

$$\omega=|\omega_B\pm n\omega_s|<\omega_s/2 \qquad (n=1,2,\ldots) \tag{4}$$

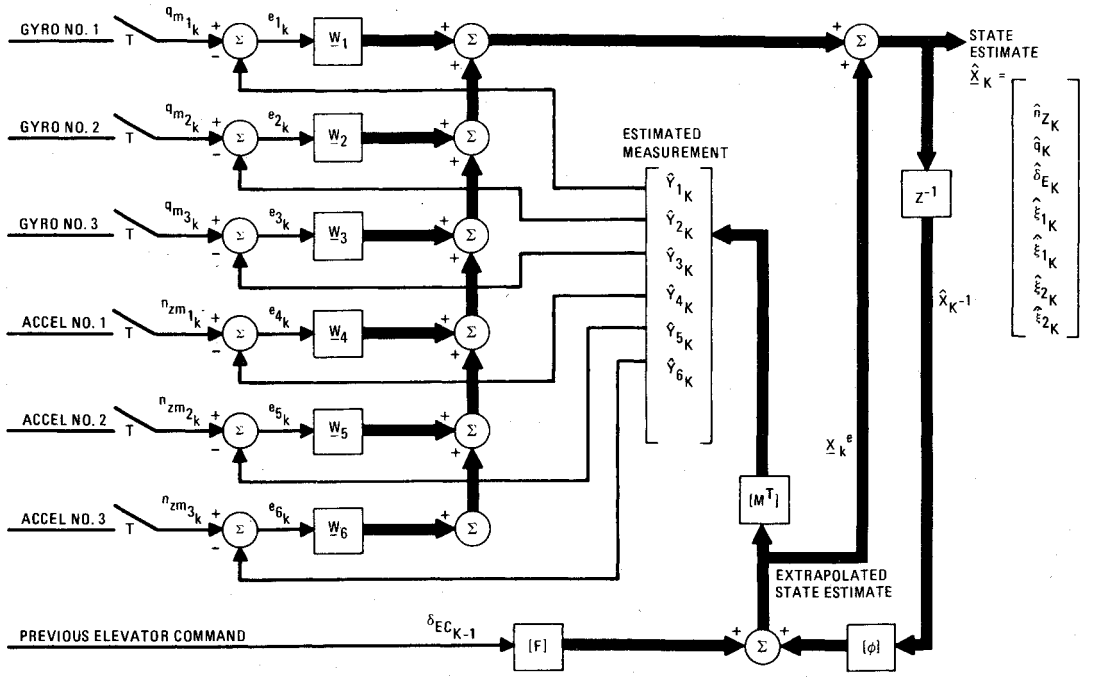

Fig. 1 Six-measurement estimator.

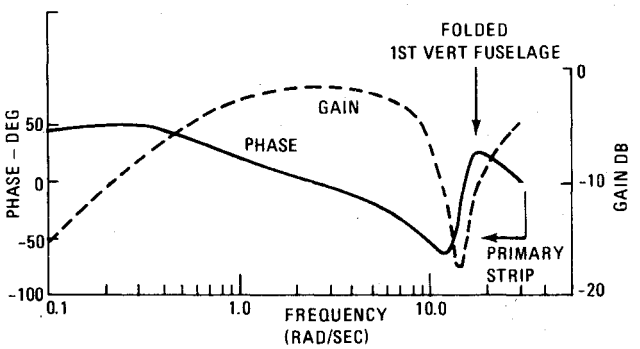

Fig. 2 Kalman estimator gain and phase vs frequency from pitch rate measurement at nose to pitch rate estimate.

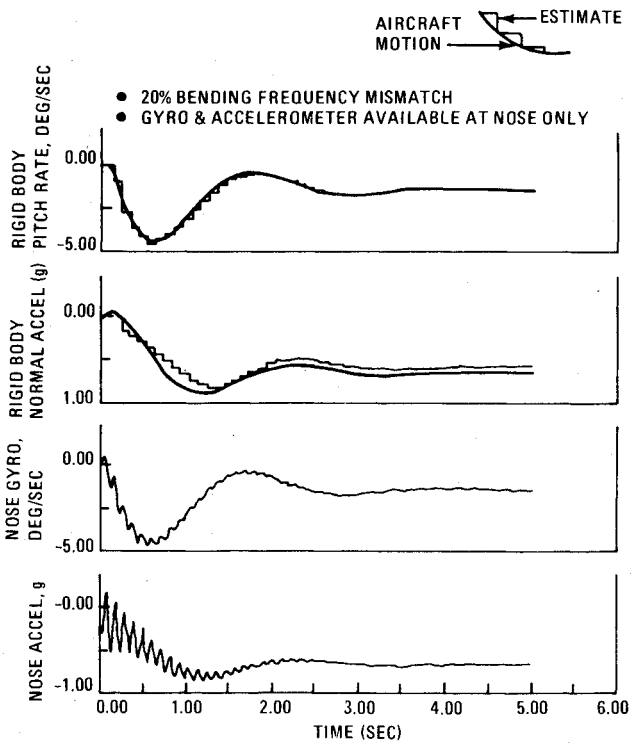

Fig. 3 Response to one-degree elevator step.

where ω_B is the original damped natural frequency outside the primary strip.

Specifically, corresponding to this example, the original bending mode damped natural frequencies are 33.4 rad/s (1st wing symmetric) and 48.5 rad/s (1st vertical fuselage). The resulting folded frequencies are 29.4 rad/s and 14.3 rad/s. Therefore, the digital filter must be designed to attenuate the bending signals at and around these folded frequencies. Recall that each bending mode has inherent structural damping so that the goal is to avoid interacting with these modes, thus permitting natural damping. As a consequence of the Kalman filter design, the correct notching characteristics are obtained. For example, the resulting gain and phase characteristics from the nose rate gyro to the pitch rate estimate are shown in Fig. 2. Note the deep notch located at the folded first vertical fuselage bending frequency. Furthermore, the resulting attenuation of the wing bending mode is not nearly as large because the flexible rates at the nose are relatively small due to wing bending. The gain characteristics associated with the wing sensor, however, exhibit significant attentuation around the folded wing bending frequency. Although the particular gain characteristics in Fig. 2 have significant low-frequency attenuation, it is compensated by the other sensor inputs and by the actuator command relationship to the rate estimate. Although the sampling frequency is less than twice either of the bending mode frequencies, Shannon's sampling theorem is not being violated. Remember, the purpose of the filter is simply to avoid interacting with the bending modes and not to reconstruct the signal. Since the filter can accomplish its goal by operating on the folded frequencies, there is no need to overburden the computer by using a faster sampling rate. For more detail concerning the appropriate criteria for choosing a sampling rate refer to Refs. 1-3.

With regard to filter performance sensitivity to uncertainties and external disturbance, simulation tests were performed with the following errors and disturbances: 20% bending frequency error, 20% mean aerodynamic chord error

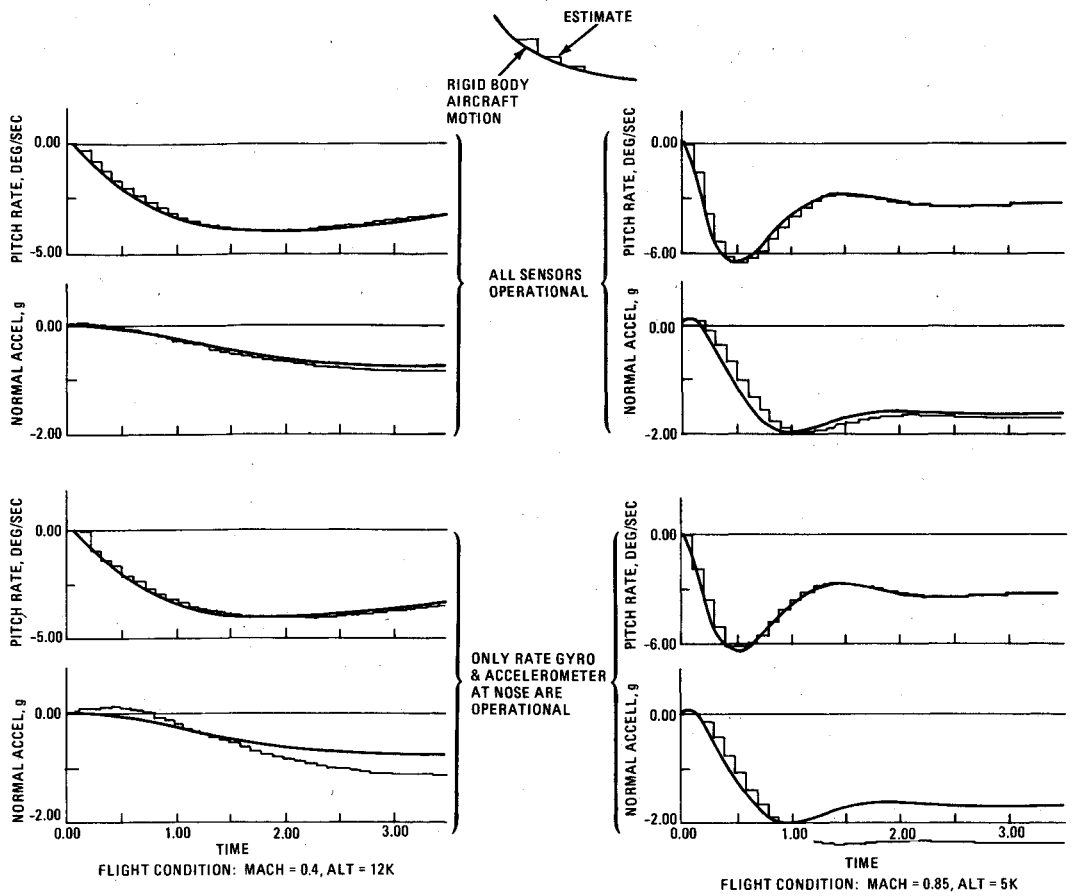

Fig. 4 One-degree elevator step response performance degradation due to flight condition uncertainties (design flight condition: Mach = 0.85, alt = 23,000 ft).

in c.g. location, 10% nondimensional stability derivative errors, 100% dynamic pressure error, and clear-air turbulence.

The first three error conditions resulted in negligible estimator performance degradation with all sensors operational. It was not until multiple sensor failures were introduced that a slight degradation was observable (see Fig. 3). Performance tolerance to gross dynamic pressure errors, which is representative of an air data system failure, is illustrated in Fig. 4. Significant errors are observed when the nose sensors only are available. It is emphasized that the latter condition would only exist following the loss of the air data system plus four motion sensors. Table 1 provides an indication of adequate estimator accuracy in the presence of turbulence.

Nondispersed Three-Fail Operational Sensor System

The development of the three-fail operational (3-FOP) sensor system started from a typical, state-of-the-art, FBW sensor system, based on the results of a previous study.[4] The set of sensors deemed typical includes: one inertial navigation system (INS), three lateral accelerometers, six skewed rate gyros, and two air data systems. Air data systems are included as part of the flight control system sensor set for flight condition identification or gain scheduling. The skewed rate gyros might be considered atypical; however, the system has been fully evaluated[5] and was recently flight tested. Since the application is for an advanced aircraft with possibly negative static stability, it is assumed that the flight control system is not operational unless all required feedback signals are available. A set of previously derived baseline aircraft three-axis digital control laws will be used for demonstration purposes. The required aircraft longitudinal motion feedback signals are n_z (normal acceleration at c.g.), q (pitch rate), and $\dot{q}$ (pitch acceleration); the required lateral/directional feedbacks are ϕ (bank angle), p (roll rate), r (yaw rate), and n_y (lateral acceleration at c.g.).

In order to achieve the goal of 3-FOP, a reconfigurable steady-state Kalman estimator is used to provide a source of analytic redundancy. Specifically, there are ten configurations derived, four longitudinal and six lateral/directional, for each of six flight conditions within the flight envelope, along with a constant parameter estimator to accommodate loss of air-data information, which constitutes two failures due to INS velocities offering an analytic redundant source. The estimator is reconfigured as a function of sensor failures, as shown in Table 2. As long as there are no more than three sensor failure combinations, there is an estimator configuration available to provide estimates of all the required feedback signals previously mentioned. It should be noted that the failure tolerance of an individual feedback signal, without analytic redundancy, varies from zero- to two-fail operational.

Table 1 Estimator accuracy in turbulence[a]

	Estimate accuracy (1 sigma)	
Sensors failed	N_z, g	q, deg/s
None	0.009	0.06
1 Pair (1 gyro & 1 accelerometer) – on wing	0.026	0.083
2 Pair – on wing and tail	0.0116	0.114

[a] Disturbance results in 1 sigma variations of 0.3g and 1.9 deg/s.

Table 2 Estimator configuration as a function of sensor failure state

Configuration		Sensor failure	Motion sensor measurements
Longitudinal	1-P	zero, or 1-norm acc	n_{zm_1}, n_{zm_2}, q_m
	2-P	2-norm acc's	n_{zm_1}, q_m
	3-P	3-norm acc's	q_m
	4-P	3-gyros	n_{zm_1}, n_{2m_2}
Lateral directional	1-L	zero, or 1-lat acc	$\phi_m, n_{ym_1}, n_{ym_2}, p_m, r_m$
	2-L	2-lat acc's	$\phi_m, n_{ym_1}, p_m, r_m$
	3-L	3-lat acc's	ϕ_m, p_m, r_m
	4-L	3-gyros	$\phi_m, n_{ym_1}, n_{ym_2}$
	5-L	INS, and zero or 1-lat acc	$n_{ym_1}, n_{ym_2}, p_m, r_m$
	6-L	INS, and 2-lat acc's	n_{ym_1}, p_m, r_m
Constant parameter		Air data plus any combination of above	Corresponding to particular sensor failure combination

In addition to the feedback states, the estimator provides estimates of surface position to account for actuator dynamics, and an estimate of elevator trim. An estimate of elevator trim is required to avoid large steady-state errors. The trim estimate is accomplished by assuming the total elevator command is comprised of a trim term, modeled as a random walk sequence, plus a perturbation elevator command term.

In order to accomplish failure detection, isolation, and reconfiguration of the motion sensors, the estimator is combined with comparison monitoring algorithms for the skewed gyros and the in-line accelerometers to form a 3-FOP sensor redundancy data management (RDM) software system. The gyro RDM algorithms[5] and the accelerometer RDM algorithms consist of voting and transient failure routines for quick removal of failed or poor sensors, and a failure detection/isolation routine to declare permanent failures. Thresholds for transient failures are based upon predicted maximum aircraft transient maneuvers; thresholds for permanent failure declarations are selected to minimize false and missed alarms based upon a statistical model of sensor performance.[5] Permanent failures are declared when filtered and rectified signal differences exceed the thresholds for a specified number of consecutive iterations.

A description of how the sensor RDM system achieves 3-FOP for the required feedback signals is now presented.

Rotational Rates

The skewed gyro comparison monitoring algorithms will derive orthogonal rates as long as no more than two gyros have failed. It will also detect a third gyro failure, at which time the estimator configuration is switched to 4-P and 4-L to derive rotational rates based on the remaining measurements.

Linear Accelerations

The first accelerometer failure is detected/isolated via comparison monitoring of the three accelerometers. Following isolation of the first failure, comparison monitoring is performed on the two remaining accelerometers, with estimated acceleration as a third signal source. At the first indication of a suspected second failure, the questionable accelerometer is removed as an input to the estimator to avoid corrupting future estimates. In turn, the estimator configuration is temporarily switched to 2-P or 2-L. Permanent reconfiguration of the estimator occurs only following a permanent failure declaration. Following the isolation of a second failure, the remaining accelerometer output is compared to the estimator output. At the first indication of a suspected third failure, the accelerometer is removed as an input to the estimator, and the estimator configuration is temporily switched to 3-P or 3-L. A permanent declaration of a third accelerometer failure will result in a permanent reconfiguration of the estimator with acceleration derived based on the remaining measurements.

Bank Angle

The primary source for bank angle information is the INS. An INS failure indication will trigger a reconfiguration of the lateral/directional estimator to either 5-L or 6-L, dependent upon accelerometer failure status. INS failure detection is assumed to be self-contained within the INS. Estimator configurations 5-L or 6-L will derive bank angle based upon the remaining lateral/directional measurements.

Pitch Acceleration

The only source of pitch acceleration is the longitudinal estimator. The estimator will be operational, provided no more than three motion sensors have failed.

It should be noted that in the event of an air data failure, a constant parameter estimator is provided, which is reconfigured as a function of motion sensor failures, as described above.

Dispersed 3-FOP Sensor System

The dispersed sensor system utilizes the same sensor set as the nondispersed, 3-FOP configuration, i.e., triplex lateral and normal accelerometers, six skewed rate gyros, air data, etc. Survivability could be optimized if it were practical to locate each of these components separately, with the maximum possible distance between them. Consideration of maintainability and packaging constraints, however, suggests fewer locations and requires easy accessibility to the components. Therefore, the gyros and accelerometers were located in three groups. Each group contains two skewed gyros in a package and two accelerometers (one normal and one lateral) also packaged together. These groups were located in the baseline aircraft so as to achieve a factor of safety of 1.5 times the 86-in. separation distance suggested by a vulnerability analysis of the system.[6] Figure 5 shows these locations relative to the aircraft center-of-gravity; their exact placement is given in Table 3.

A vulnerability analysis examined the relative differences in survivability of three sensor configurations. These were the nondispersed baseline sensor configuration, the nondispersed 3-FOP sensor system, and the dispersed 3-FOP sensor system The hostile threat weapons investigated were the 12.7 mm armor piercing incendiary (API), and the 23 and 37 mm high explosive incendiary (HEI) projectiles. The results of the vulnerability analysis are summarized in Table 4; Ref. 6 provides additional details.

In order to accommodate the dispersed gyros and accelerometers, sensor normalization must be added to the

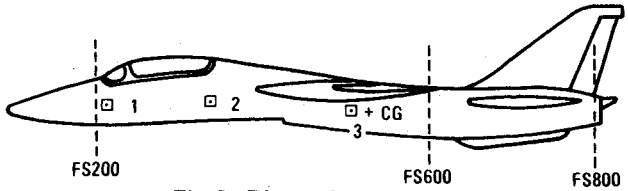

Fig. 5 Dispersed sensor locations.

Table 3 Dispersed sensor locations

Two pack pair location	Fuselage station, in.	Water line, in.	Butt line, + right in.
1	210	140	−3
2	339	145	−2
3	506	137	+6
Nominal c.g.	524	145	0

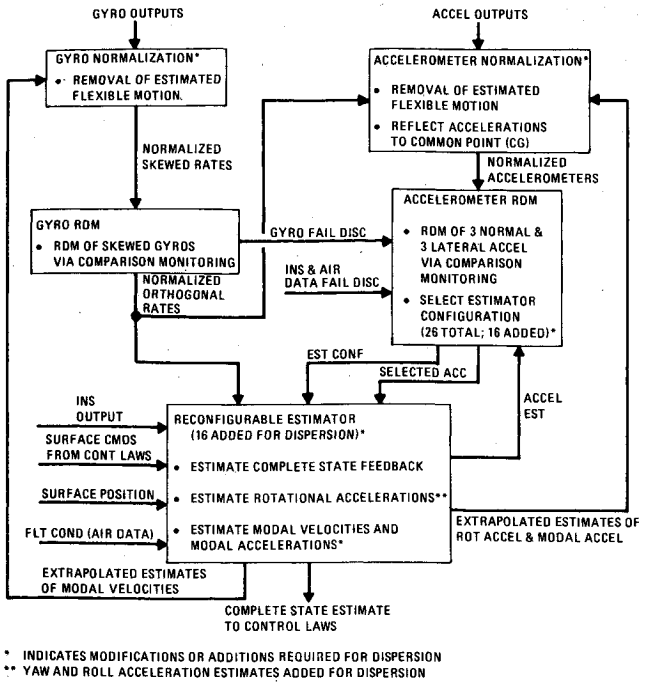

Fig. 6 Dispersed 3-FOP sensor RDM data flow.

nondispersed sensor RDM algorithms. The normalization approach is the same, in concept, as previously described. Specifically, the nondispersed estimator equations are augmented to provide estimates of modal rates $\hat{\dot{\xi}}$ and accelerations $\hat{\ddot{\xi}}$ to be used for bending compensation, as well as estimates of yaw acceleration $\hat{r}$ and roll acceleration $\hat{p}$ to compensate for kinematic effects. The data flow of the sensor RDM algorithms is shown in Fig. 6. It is noted that sensor normalization is performed prior to comparison monitoring; that is, once the normalization process is complete, the RDM algorithms operate as if there is no dispersion. The normalization equations implemented for four bending modes are as follows.

The normalized skewed gyro signals (ω_{s_i}) are given by

$$\omega_{s_i} = \omega_i - B_i \sum_{j=1}^{4} \psi_j^i \hat{\dot{\xi}}_j^e \tag{5}$$

where ω_i is the two-element vector of sensed rate for the sensors at position i, $\hat{\dot{\xi}}_j^e$ is the extrapolated estimate of the jth modal rate, ψ_j^i is the assumed jth mode slope vector (3×1) at location i, and B_i is the constant transformation matrix to two-pack coordinates from orthogonal control axes.

The normalized lateral and normal accelerometer signals (n_{ym}^i, n_{zm}^i) are given by

$$n_{ym}^i = n_y^i - \sum_{j=1}^{4} y_j^i \hat{\ddot{\xi}}_j^e - [lx_i(\hat{r}^e + q_m p_m) + lz_i(q_m r_m - \hat{p}^e) - ly_i(p_m^2 + r^2{}_m)]$$

$$n_{zm}^i = n_z^i - \sum_{j=1}^{4} z_j^i \hat{\ddot{\xi}}_j^e + [lx_i(p_m r_m - \hat{q}^e) - lz_i(p_m^2 + q_m^2) + ly_i(\hat{p}^e + q_m r_m)] \tag{6}$$

where n_y^i, n_z^i are the sensed lateral and normal acceleration at the ith location, $\hat{\ddot{\xi}}_j^e$ is the extrapolated estimate of the jth modal acceleration, y_j^i, z_j^i are the jth mode shape displacements in the y and z directions at location i, lx_i, ly_i, lz_i define the ith location relative to the nominal c.g., p_m, q_m, r_m are the normalized orthogonal rates, and $\hat{p}^e$, $\hat{q}^e$, $\hat{r}^e$ are extrapolated rotational acceleration estimates.

Referring to Fig. 6, the inputs to the reconfigurable estimator are established as a result of comparison monitoring of the normalized sensor signals. Another way of interpreting the normalized signals is to view them as estimator residuals plus the rigid body extrapolated state estimate at the nominal c.g. location. Therefore, comparison of normalized signals is equivalent to comparison of estimator residuals.

Each nondispersed estimator configuration requires additional subconfigurations, or additional sets of Kalman weights, to accommodate the different combinations of sensors that are selected by comparison monitoring as inputs to the estimator. If a separate configuration was needed to accommodate each possible sensor combination, a total of 306 configurations would be required. However, a prudent appraisal of each nondispersed estimator configuration has led to a requirement for a total of 26 dispersed estimator configurations. Specifically, all nondispersed configurations, except 4-P and 4-L, will have three subconfigurations to accommodate all possible accelerometer combinations. Estimator configurations 4-L and 4-P, which do not use any accelerometer measurements, will require no subconfigurations. The basic approach to reducing the number of estimator configurations was to assume, for estimator synthesis, that all bending information was contained only within the accelerometer measurements for all configurations that use accelerometer measurements. During the design process for these configuations, bending that is corrupting the gyro measurements is accounted for by increasing the gyro measurement noise. Corresponding to estimator configurations that are used in the event of a failure of all the accelerometers, e.g., configuration 4-L or 4-P, it is reasonable to assume that all the gyros are available. Therefore, only one estimator configuation is needed for this condition; specifically, for this condition the gyro RDM will always select gyro pairs (3, 4) and (5, 6), and the estimator has been designed accordingly, using a bending model corresponding to these particular gyro pairs.

Sensor normalization equations [Eqs. (5) and (6)] include nonlinear kinematic effects as well as coupling from all four bending modes, i.e., first fuselage vertical bending (7.63 Hz, $j=1$), first wing symmetric bending (4.4 Hz, $j=2$), first lateral fuselage bending (8.9 Hz, $j=3$), and first antisymmetric wing bending (5.36 Hz, $j=4$). The steady-state Kalman weights were derived using only the linear kinematic terms, the symmetric bending modes (i.e., $j=1,2$), for longitudinal estimation, and the antisymmetric modes (i.e., $j=3, 4$), for lateral/directional estimation.

The algorithms to implement the functions depicted in Fig. 6 were combined with the previously noted three-axis digital control laws, within a six-degree-of-freedom nonlinear simulation of the baseline aircraft. These algorithms required approximately 20K words of storage, of which 10K were constants to accommodate six flight conditions. Verification testing is described in the following section.

Dispersed 3-FOP Sensor System Verification Testing

Accelerometer and gyro failure models were introduced into the simulation to evaluate the system's capability to normalize the signals, detect and isolate the failures and to automatically reconfigure the system while operating in steady-state flight, maneuvering flight, turbulence, and during maneuvers in turbulence. System performance was evaluated in response to the following sensor failures: hardover failures (i.e., 110 deg/s for gyros, 10g for normal accelerometers, 1g for lateral accelerometers), failures to zero, high bias errors (i.e., 5 deg/s for gyros, 0.5g for normal accelerometers, 0.3g for lateral accelerometers), high scale factor errors (i.e., 50% scale factor errors), high noise (i.e., 3σ

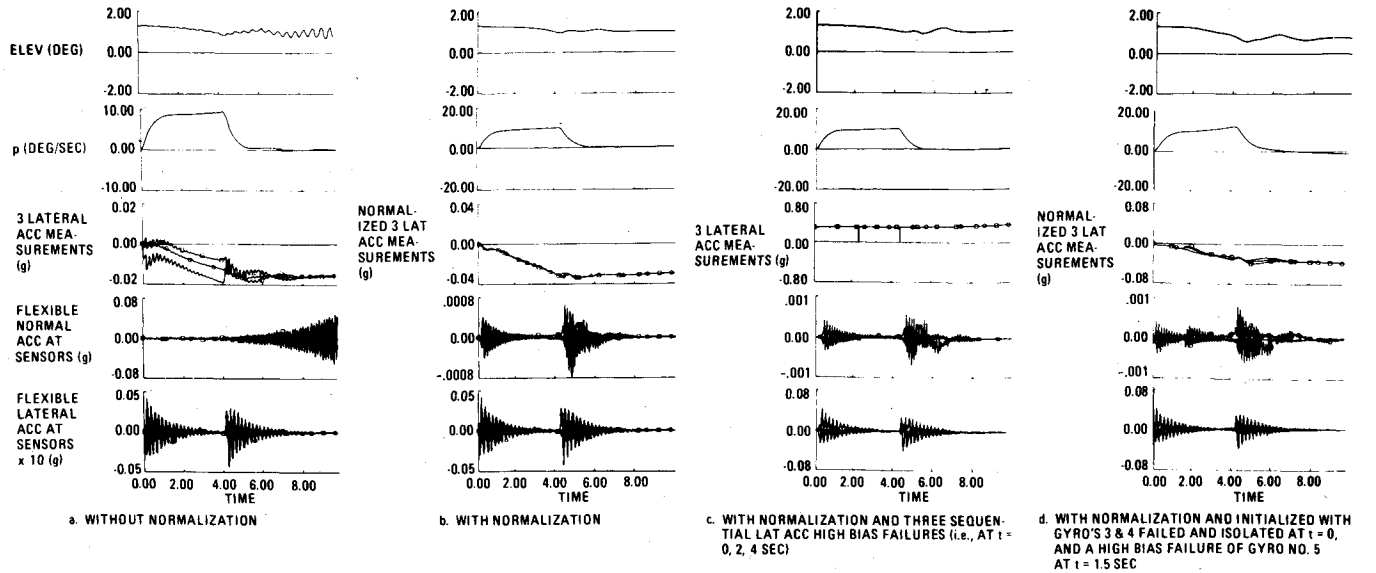

Fig. 7 Level turn maneuver at Mach = 0.625, alt = 33,000 ft.

Table 4 Vulnerability results – single hit probability of kill, $P_{k/H}$

Weapon	Baseline sensor system (no dispersion & no analytic redundancy)	3-FOP, non-dispersed sensor system (analytic redundancy)	Dispersed sensor system (dispersion & analytic redundancy)
37 mm	3.2%	0.6%	0
23 mm	2.0%	0.04%	0
12.7 mm	0.4%	0	0

failure noise levels were 15 deg/s for gyros, 5*g* for normal accelerometers, 1*g* for lateral accelerometers), INS failure detected and isolated, and air-data failure detected and isolated.

During most test runs, multiple sensor failures were inserted sequentially so as to minimize the number of runs while fully assessing the redundancy management system's capability. Simulated maneuvers, initialized at several different flight conditions within the flight envelope, included pull-ups, level turns, and snap rolls. With few exceptions, the test results demonstrated the system's capability to successfully normalize the sensor signals, detect and isolate failures, and to properly reconfigure the sensor system with unobservable failure transients. During all failure test cases, all flexible motion was successfully filtered with virtually no structural interaction with the rigid-body control laws. As long as air-data information was available for gain and estimator parameter scheduling, there was no handling quality degradation until a third gyro failure or a third accelerometer failure. The degradation following a third failure was slight, in that level I handling qualities (as per MIL-F-8785B) were retained.

Figure 7 shows simulation results of selected level turn test runs. The level turn maneuver is a three-axis maneuver that consists of a 4 s roll rate command (10 deg/s) to achieve approximately a 40-deg bank angle, a yaw rate command to help coordinate the turn, and a pitch rate command to maintain level flight. Figure 7a demonstrates the need for sensor normalization. Specifically, without normalization, the figure shows unstable longitudinal control resulting from elevator control interaction with sensed flexible motion. Figure 7b shows results with sensor normalization, and with the dispersed 3-FOP sensor system fully operational. Two important observations are made: first, the flexible motion, although excited, is allowed to damp naturally; second, normalization is nearly perfect, as demonstrated by the normalized lateral acceleration measurements as compared to the actual measurements. Figure 7c shows the system's response to three sequential lateral accelerometer bias failures. Table 5 lists time keyed significant events corresponding to this test run. Note that at 4.1 s into the run, the control laws were operating without lateral accelerometer measurements, estimating lateral acceleration via the remaining measurements. All flexible motion was naturally damped without control interaction. Figure 7d shows results in response to the loss of rate gyro information. The test was initialized with gyros nos. 3 and 4 failed and isolated. At 1.5 s into the test run gyro no. 5 was failed. At 1.6 s all gyro measurements were eliminated via the gyro RDM, and the estimator was reconfigured. A permanent failure declaration occurred at 2.8 s. Once again, all flexible motion was normalized successfully, as demonstrated by the normalized accelerometer traces and the absence of any control interaction.

Table 5 Significant events in response to three sequential lateral accelerometer failures (Fig. 7c)

Time, s	Significant event
0	Acc no. 1 failed
0.1	Acc RDM temporarily eliminates acc no. 1 thru voting
0.9	Acc no. 1 isolated as permanent failure
2.0	Acc no. 2 failed
2.1	Acc RDM temporarily eliminates acc no. 2 thru voting; estimator configuration switched to 2-L
3.0	Acc no. 2 isolated as permanent failure
4.0	Acc no. 3 failed
4.1	Acc RDM temporarily eliminates acc no. 3 thru voting; estimator configuration switched to 3-L
5.1	Acc no. 3 isolated as permanent failure

Two problems were encountered during testing that would most likely require changes to the sensor RDM system. The first problem was the system's inability to detect lateral accelerometer failures to zero. This was due to characteristically low lateral acceleration levels during the test maneuvers. Built-in tests probably would be required to overcome this problem. The second problem involves a significant degradation in closed-loop performance with the complete loss of air data. In order to compensate for loss of air data, the approach was to select a set of constant estimator parameters that would result in satisfactory performance throughout the flight envelope. This approach worked well without aircraft bending. Augmenting the aircraft equations with highly coupled bending equations resulted in instabilities at certain high dynamic pressure flight conditions. Further adjustments to the constant parameters eliminated these instabilities; however, other flight conditions then exhibited significantly underdamped longitudinal characteristics, i.e., of level III quality. It is conceivable that a set of fixed parameters exists that would further improve the flying qualities. Other possible alternatives would be to attempt to identify the flight condition via flight control measurements, to utilize additional analytic redundancy techniques, or to reconfigure the control laws.

Conclusion

The combat survivability of a fly-by-wire sensor system can be significantly enhanced through the use of dispersion and/or analytic redundancy. Both of these techniques have been utilized with a state-of-the-art conventional sensor set. The result has been improved survivability and failure tolerance without the use of additional sensors.

A reconfigurable steady-state Kalman estimator was used to accomplish both the analytic redundancy and the normalization of dispersed sensor signals. A practical, three-fail operational integrated sensor hardware/software system has been formed by combining the estimator with conventional comparison monitoring techniques and a set of flight control sensors whose failure tolerance varies from zero- to two-fail operational without analytic redundancy. Simulation results supported the practicality of this approach by demonstrating the estimator performance (i.e., sensor normalization and analytic redundancy performance) to be relatively insensitive to "real world" disturbances and reasonable parameter uncertainties.

Corresponding to the loss of flight condition (air data) information, which constitutes at least two failures in this system, good flying qualities were obtained using non-dispersed sensors. However, for the dispersed sensor system, level III flying qualities occurred. The flying quality degradation is due to the estimator being the sole source of certain control feedback signals. Improvement can be realized using one of several alternatives, which require further investigation.

Acknowledgments

This work was partially supported by the Air Force Flight Dynamics Laboratory, Wright-Pattrson AFB, Ohio, under Contract F33615-77-C-3041.

References

[1] Berman, H. and Gran, R., "Design Principles for Digital Autopilot Synthesis," *Journal of Aircraft,* Vol. 11, July 1974, pp. 414-421.

[2] Berman, H., "Digital Control System Synthesis and Laboratory Verification for Fly-By-Wire System Applications," Grumman Aerospace Corp. Report ADR 01-03-76.4, Aug. 1976.

[3] Powell, J. and Katz P., "Sample Rate Selection for Aircraft Digital Control," AIAA Guidance & Control Conference, Aug. 1974.

[4] Boudreau, J., "Impact of CCV Requirements on Flight Control System Design," *Journal of Aircraft,* Vol. 14, Nov. 1977, pp. 1051-1059.

[5] Weinstein W., "Development of an Advanced Skewed Sensory Electronic Triad (ASSET) System for Flight Control," NADC-76295-30, Oct. 1976.

[6] Berman, H., Boudreau, J., "Improved Combat Survivability for Fly-By-Wire Sensor Systems, AIAA Paper 78-1277, AIAA Guidance and Control Conference, Aug. 1978.